Choice of the Stress Integration Scheme for Accurate Large-Deformation Finite Element Analysis

Fabrizio Antonio Stefani*, Mattia Frascio, C.A. Niccolini Marmont Du Haut Champ

Department of Mechanical Engineering, Energetics, Management and Transportation (DIME), Polytechnic School - University of Genoa, Via Opera Pia, 15A, Genoa, Italy 16145

* Corresponding author. *E-mail address*: stefani@unige.it (F. Stefani). ORCID: 0000-0001-5625-987X

Abstract

The use of computational structural models that include geometrical non-linearity in many application cases may require high reliability in prediction of displacements. Nevertheless, large differences up to 60% on maximum total displacement have been found among results of static large-deformation analyses performed by means of the major commercial software packages in a simple benchmark study with linear material properties. In order to investigate the causes of such disagreement, the present work compares different finite element formulations including well-established stress update schemes. The various formulations are tested, and results are compared in three test cases. Rodriguez stress update algorithms have shown the best performance among methods reported in literature. Finally, the cause of the large differences found in the predictions of commercial codes is identified. It is linked to the energetic inconsistency of some stress update methods in the simulation of extension/compression loading conditions. Such inaccuracy is reproduced analytically by formulating and integrating the corresponding inconsistent constitutive equations. The identified problem is very important for designers, as it affects almost all the static simulations, which are the most common type of large-deformation analyses and usually involve extension/compression loading.

Keywords: Finite element analysis; geometrical non-linearity; large deformation; stress update; objectivity; work conjugacy

1 Introduction

In large deformation analysis [1], the stress integration scheme affects both the accuracy of computation and the convergence of the solution [2]. Therefore, choice and formulation of the particular stress update procedure for a specific application are an important issue, which has been extensively studied in literature. As an example, the works [2–6] are related to large deformation simulations of hardening materials as well as unsaturated soils in geomechanics, plastic and homogeneous anisotropic hardening materials in sheet metal forming processes.

The present work is mainly aimed to compare the accuracy relevant to both displacement and stress predictions of large-displacement analysis methods that use different stress integration algorithms. Special reference is made to well-established stress update methods and, particularly, to those potentially employed in the major commercial codes according to [7]. Such methods and suitable variants are implemented in an ad-hoc finite element code, capable of easily switching the different methods. It takes advantage of the *FEMLub* library, developed in order to study multi-disciplinary problems where tribology and structural phenomena interact, i.e. elasto-hydrodynamic lubrication. Since in such field the reliability of displacement predictions is particularly important, the present work is aimed to achieve high accuracy in structural model computations. The Lagrangian formulation (LFM) of the problem is used together with the updated-Lagrangian (UL) method [1]. It is derived from its Eulerian counterpart as presented in [7] for different stress rates in order to fulfil the requirement of work conjugacy and consistency of stress/strain choice and corresponding constitutive model.

In the following, the analyzed stress integration methods [1,8–13] are briefly recalled in Paragraph 2, and proper variants devised during the development phase are classified. Particularly, algorithms based on a corotated configuration [11,14–16] and their possible variants deduced from literature are more deeply analyzed, since we have found that a comprehensive treatise describing these algorithms [16] requires more details in order to adapt the procedures to the UL approach. As far as applications are concerned (Paragraph 3), simple benchmark static analyses with both traction and bending loads are performed in Paragraph 3.1 by means of popular commercial programs that employ different stress integration methods. Large differences in displacement and stress predictions of the various codes due to the use of different stress-update algorithms are assessed in the traction load case. In order to explain such unexpected result, the stress predictions of both the considered stress integration algorithms implemented in *FEMLub* code and the chosen commercial codes are compared by means of three stress integration tests allowing analytical solution in Paragraph 3.2. Namely, the *extension-compression* as well as *extension-rotation* tests proposed in [13] and the *simple shear* test used in [7,12,16] are chosen to include the most common strain conditions. Analyzing the results of the stress integration tests allows us: to choose the most accurate stress update algorithm; to infer a qualitative correlation between different stress integration schemes and results; to explain the above-cited inconsistency of some algorithms in the simulation of extension/compression loading conditions. Afterwards, such inconsistency is simulated analytically in order to reveal its nature in Paragraph

3.3. The initial analysis is finally repeated by using the most accurate stress integration method encoded within *FEMLub* and its results are compared with the reference ones of the commercial codes in Paragraph 3.4.

2 Theoretical models

The following section cites the mathematical models used in the present work for static structural analysis of large-deformation problems concerning linear elastic material. Special reference is carried out to stress integration and work-conjugacy [17–19].

Firstly, the FE Lagrangian formulations of the related equilibrium problem [1,8] are retrieved from the Eulerian forms of the principle of virtual work [7] in terms of the following objective stress rates: Truesdell rate of Cauchy stress (TC), Biezeno-Hencky rate of Cauchy stress (BC) and Jaumann rate of Cauchy stress (JC).

Different "classic" methods for stress update are coupled with the proper corresponding formulation of the equilibrium equations. The simplest stress integration approach, referred to as *Bathe linear* and proposed in [8], relies on Euler step as well as linearized strain increment. Such integration method is used in conjunction with TC formulation. It has been updated (*Bathe* method, [1]) by using the Green-Lagrange strain increment as explained in [3].

The classic *Hughes-Winget* [9] stress update method, coupled to the JC formulation, takes advantage of Jaumann objective stress rate and a transformation based on geometrical concepts at the mid-time step, in order to keep the incremental objectivity of the integration procedure.

Differently, in the *Gadala-Wang* method [10] for the TC formulation the transformation is carried out by means of Truesdell objective stress rate. While such method considers the linearized strain increment, an alternate approach, referred to as *Gadala-Wang non-linear*, is tested here by resorting to the whole Green-Lagrange strain increment.

In the explicit *Pinsky* integration scheme reported in [11] the same transformation used in *Gadala-Wang* approach for current stress is applied to both current stress and stress increment.

Two stress update algorithms named *Rodriguez 1* and *Rodriguez 2* [12,13] take advantage of the family of transformations defined in [11]. In order to correctly capture the inherent non-linear behavior of large displacements, the former algorithm computes the stress increment by including quadratic terms in Green-Lagrange strain, while the latter employs the mid-point rule like the *Hughes-Winget* method and the linearized stress increment.

Notice that both *Rodriguez 1* and *Pinsky* methods take advantage of the same transformation, but they are different in that the former method includes non-linear strain terms in order to predict stress increment while the latter uses linearized strain. In addition, *Rodriguez 1* is also different from *Gadala-Wang non-linear*. Indeed, although both methods include non-linear strain terms, *Gadala-Wang non-linear* method does not transform the stress increment, differently from *Rodriguez 1*.

Methods based on a Corotated Configuration (CC) exploit corotational objective stress rates like Green-Naghdi and Zaremba-Jaumann ones. They use a rotation-neutralized configuration that co-rotates with the body, i.e. it is not affected by relative rigid motions. After the related quantities are transformed in such configuration, the constitutive equation is integrated, and the obtained results are rotated back in the updated configuration. Several works deal with this topic, e.g. [11,14,15], and comprehensive explanation of the working principle of such methods is found in [16], particularly for the algorithms developed by Hughes [14] using Green-Naghdi and Zaremba-Jaumann stress rates, in the present work referred to as *Hughes-Green-Naghdi* and *Hughes-Zaremba-Jaumann*. Nevertheless, the description of these algorithms reported in [16] is unspecific and their implementation in the UL framework needs an additional expedient. The required adjustment assumes that in the UL method the current spatial frame (at time t) is used as rotation-neutralized configuration. Accordingly, the transformations of spatial deformation to its material counterpart and of the resulting stress to the new time step configuration differ from the corresponding relationships found in [16] in that the incremental rotations are used instead of the total ones.

In both algorithms the total deformation gradient at the middle time step $\mathbf{F}^{t+\Delta t/2}$ is found by interpolation. Variants are devised by altering the deformation gradient computation. The *spatial Green-Naghdi* algorithm evaluates the increment of deformation gradient ${}^{t}\Delta\mathbf{F}^{t+\Delta t/2}$ from the incremental displacement derivatives computed in the current (spatial) reference. Differently, in the *material Green-Naghdi* algorithm variant $\mathbf{F}^{t+\Delta t/2}$ is computed by interpolating and deriving the displacements in the material reference system, i.e. the initial time (t = 0) configuration. Finally, in *mid-step Green-Naghdi* method the mid-time step is taken as reference system for the computation of the corresponding incremental deformation gradient, namely ${}^{t+\Delta t/2}\Delta\mathbf{F}^{t+\Delta t}$, which replaces ${}^{t}\Delta\mathbf{F}^{t+\Delta t/2}$.

3 Results

3.1 Benchmark problem solved by means of commercial software

Plane stress analysis of a square model (100 x 100 mm^2) with a thickness of 5 mm is carried out by means of commercial codes equipped with the large deformation option. The domain is discretized by means of quadrilateral isoparametric elements by dividing its sides in 30 equal parts so that a total of 961 nodes and 900 elements are obtained. The Young modulus E of the linear elastic material is 30 000 MPa while the Poisson ratio ν is 0.2. As shown in Fig. 1, the left side (x=0 mm) of the square sheet is fully constrained. Either a tractive nodal force $F_{x\,i}$ equal to 100 000 N (in the positive x direction) or a vertical one $F_{y\,i}$ equal to -30 000 N (in the negative y direction) is applied to each node i of the right side (x=100 mm) apart from the corner nodes, which are loaded by either $F_{x\,i}/2$ or $F_{y\,i}/2$ in the two simulated problems, referred to as traction and bending load cases. Therefore, the corresponding total forces imposed on the right side are $F_x = 3.0 \times 10^6$ N and $F_y = -9.0 \times 10^5$ N, as respectively plotted in Fig. 1 a) and b). Differently from

the former one, bending load case yields significant material rotations, which can involve objectivity issues.

Fig. 2 and Fig. 3 plot for each load case the maximum vector sum (L-2 norm) of displacement components and Von Mises stress bounds in the assumption of both linear and (geometrically) non-linear analysis in order to highlight possible differences among the predictions of the different codes and the relevant models. Obviously, in any case the agreement is good for the small displacement simulations, where the small differences depend on algorithmic details like the use of specific shape functions [20], reduced integration [21], B-Bar method [22], etc. Indeed, the corresponding relative variations (the size of the deviation in relation to a reference value, e.g. the mean) of maximum displacements are equal to 0.003 and 0.66 % for traction and bending load cases, respectively (since deviations are small the relative variations do not depend significantly on the reference value). On the contrary, the differences in predictions of maximum displacements relevant to large deflection simulations are particularly large for the traction load case. Precisely, while for the bending case the relative variation among maximum displacements predicted by the different codes is about 14.5 %, in the traction case the corresponding relative variation between results of *software A* and *D* is in the range 45.6-83.9 %, depending on the reference value (lower and upper bounds of the range are determined by choosing the highest and the lowest prediction as reference value, respectively). Since the result variation is high in traction load case, it is reasonable to investigate its causes.

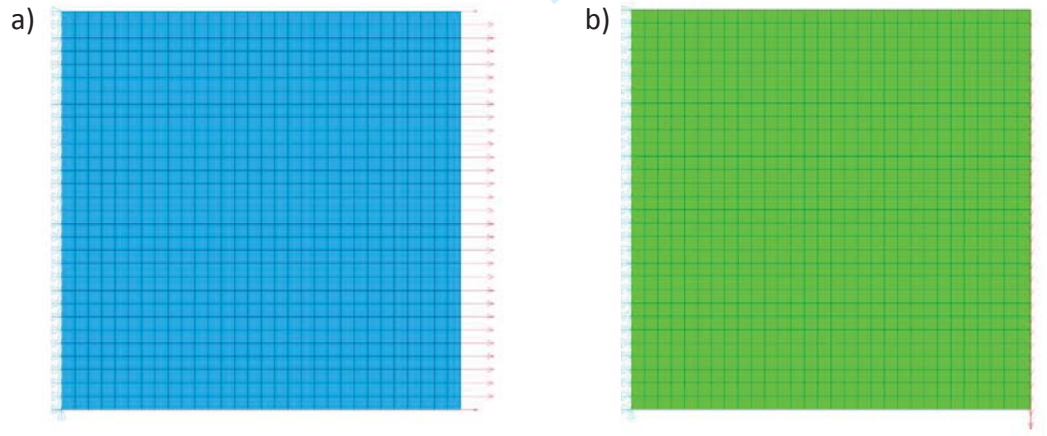

Fig. 1 Mesh, boundary conditions and loads of the benchmark problem: a) traction load case, b) bending load case.

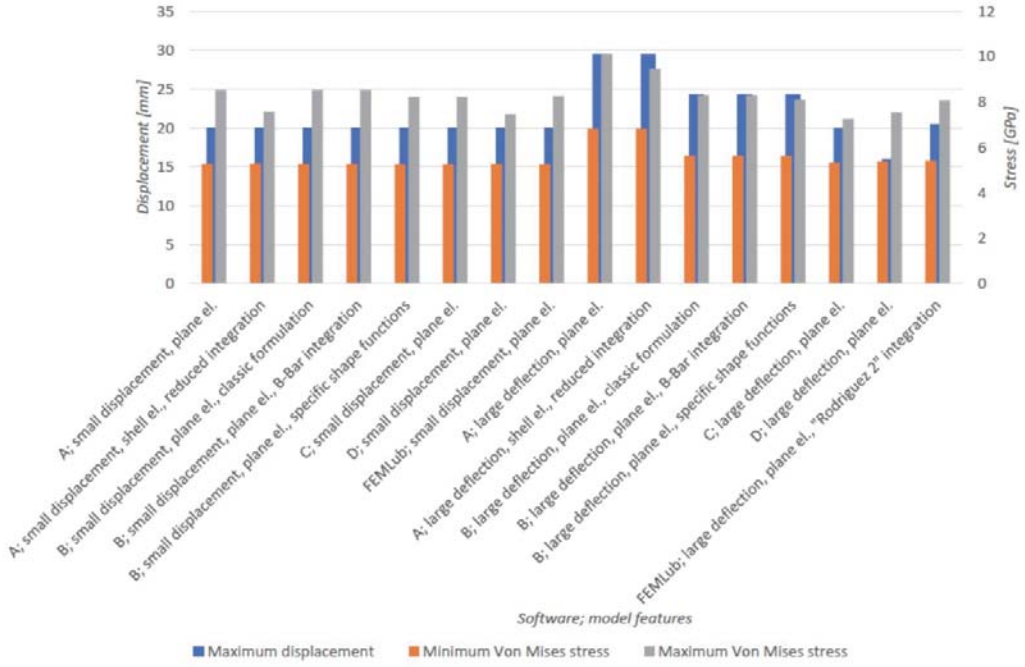

Fig. 2 Von Mises stress range and maximum displacements computed by means of different FE software and type of analysis for the benchmark traction load case.

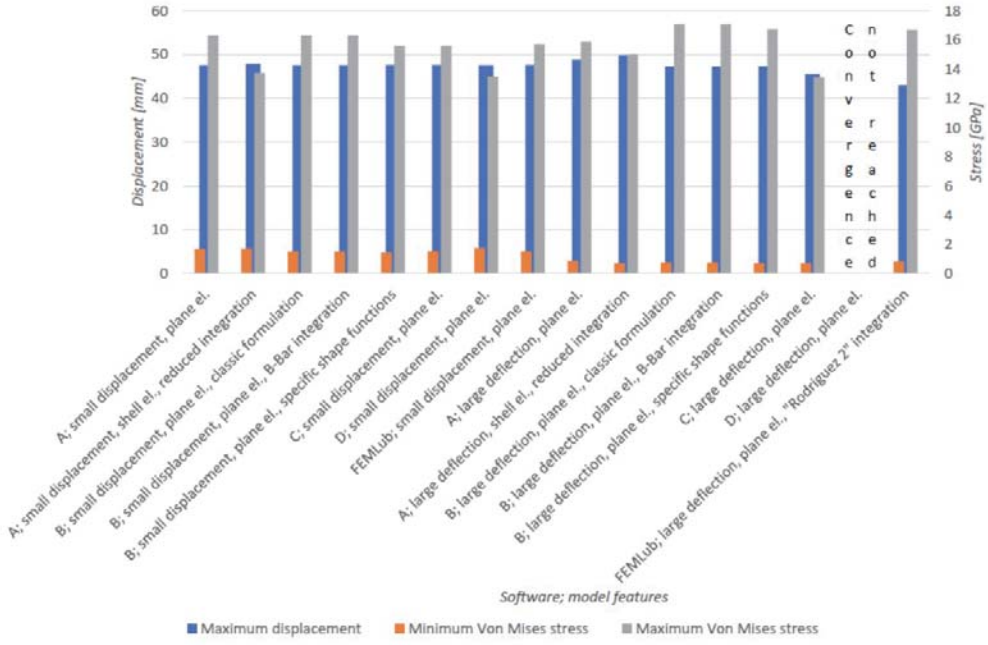

Fig. 3 Von Mises stress range and maximum displacements computed by means of different FE software and type of analysis for the benchmark bending load case.

Particularly, such relative variations are much higher in large deflection than in small displacement analysis, so that they are unlikely due to the above-cited algorithmic details solely. In addition, as in the presence of material rotations the gap between the different predictions reduces, it seems to be unrelated to the objectivity of the stress integration. Nevertheless, with the exclusion of the mentioned algorithmic details, the main differences between the different commercial codes for large deflection analysis involve the stress integration methods. Indeed, as meant by the results in [7] and information reported in the relevant theoretical manuals, the various programs take advantage of different stress integration algorithms for large deflection simulation. Particularly, *software A* employs the Jaumann rate of the Cauchy stress incorrectly matched with constant material elasticity tensor; *software B* is based on Green-Naghdi formulation; *software C* uses the Truesdell rate of Cauchy stress; more generically, *software D* takes advantage of a CC method. Accordingly, although objectivity is not the main concern, in order to find the main reasons for the differences highlighted in Fig. 2, we will go through the different stress integration strategies, as they make up the real element of difference among various codes.

3.2 Stress integration tests

Specific testing conditions are extracted from different papers, i.e. [7,12,13,16,23], so that stress integration algorithms are checked by means of three tests: *extension-compression*, *extension-rotation*, *simple shear*. They are chosen in order to include the most common motions of the structure particles, i.e. relative motions that yield extension, compression and shear combined with possible rigid rotations of the body. Particularly, the rotation motion is simulated in order to test the incremental objectivity or, better, the priority on rigid motion [12] or weak objectivity [24] of the algorithms. By a rigorous theoretical point of view, the choice of the rotation motion to test the effect on the algorithm response of all possible rigid motions is inherently non-objective. In any case, this choice is very reasonable and common in most simulations. The exact analytical solutions of the three tests are reported in [12,13,16].

In all of the tests, as in the cited Rodriguez's works [12,13], a unit square (1000 x 1000 mm^2) with unit thickness undergoes a deformation path under plane stress conditions. It is made of linear elastic material with Poisson ratio $\nu = 0$ and Young's modulus E = 1.0×10^{-6} MPa, i.e. assessed stress is relative to E. A fixed number of time steps N equal to 50 (the highest employed in the reference papers) is chosen.

The simulated "time" t (dimensionless parameter equal to the current time divided by the total simulation time) ranges between 0 and 1 in *extension-compression* as well as *extension-rotation* tests, whereas it raises from 0 to 0.9 in *simple shear* test. Therefore, the corresponding time steps Δt are equal to 1/50 and 9/500, respectively.

The proposed UL implementation of CC methods is validated and, afterwards, the tests are performed for each algorithm cited in the theoretical part. The relevant numerical data are stored in a public dataset [25] of a repository. A final consideration conveyed by the comparison of the

stress histories predicted by CC algorithms is that *Hughes-Green-Naghdi*, *spatial Green-Naghdi* and *material Green-Naghdi* algorithms are different sequences of operations that implements the same method, since the corresponding stress histories are perfectly overlapped curves in all of the three tests. This result can be easily proved mathematically. The only algorithm that takes advantage of Green-Naghdi stress rate and that is actually different from the others is *mid-step Green-Naghdi*.

Table 1. Level of agreement with the exact theory for the considered integration methods expressed by the RMS relative error Δ and highlighted by the following colours (from the worse to the best). Red - poor agreement both from qualitative and quantitative point of view (Δ greater than 140%). Orange - only qualitative agreement (Δ between 60 and 140%). Blue - imperfect quantitative agreement (Δ between 30 and 60%). Green - good agreement (Δ lower than 30%).

		RMS deviation from exact theory Δ [%] in test:		
Model type	***Model label***	**extension-compression**	**extension-rotation**	**simple shear**
Classic UL	Bathe linear	77.2022	180.2427	100.0000
	Bathe	76.0095	139.0210	100.0000
	Rodriguez 1	4.4198	4.1618	53.2338
	Rodriguez 2	0.0089	0.6845	11.0126
	Hughes-Winget	2.6689	16.4161	45.2004
	Gadala-Wang	1.1029	99.8680	13.9167
	Gadala-Wang nonlinear	$1.0650 \cdot 10^{-14}$	24.8580	34.7502
	Pinsky	3.3126	98.9769	10.2014
CC	Material Green-Naghdi	77.8015	81.4747	98.0572
	Spatial Green-Naghdi	77.8017	81.4746	98.0573
	Mid-step Green-Naghdi	79.0110	38.3884	98.0573
	Hughes-Green-Naghdi	77.8017	81.4746	98.0573
	Hughes-Zaremba-Jaumann	1.0733	2.4367	79.5921

Table 1 reports the level of agreement with the *exact theory* of the stress integration methods considered in the present study. Such assessment is performed by computing the percentage RMS deviation from the theoretical curves as follows

$$\Delta = \sqrt{\frac{\sum_{i=1}^{N}\left[\sigma_x^i - \sigma_x(t_i)\right]^2}{N\left(\sigma_x^{RMS}\right)^2} + \frac{\sum_{i=1}^{N}\left[\sigma_y^i - \sigma_y(t_i)\right]^2}{N\left(\sigma_y^{RMS}\right)^2} + \frac{\sum_{i=1}^{N}\left[\sigma_z^i - \sigma_z(t_i)\right]^2}{N\left(\sigma_z^{RMS}\right)^2}} 100 \qquad (1)$$

where σ_x^i, σ_y^i, $\sigma_{xy}{}^i$ are the Cauchy stress components numerically assessed by the method in study at time t_i; $\sigma_x(t)$, $\sigma_y(t)$, $\sigma_{xy}(t)$ are the functions of time t defined by the equations reported in [12,13,16] for the three tests according to the *exact theory*; σ_x^{RMS}, σ_y^{RMS}, $\sigma_{xy}{}^{RMS}$ are the reference values of the stress components, which are assumed equal to either the RMS value of the relevant functions $\sigma_x(t)$, $\sigma_y(t)$, $\sigma_{xy}(t)$ if it is non-zero or the maximum RMS value of the same theoretical functions otherwise.

The four levels of agreement (poor, qualitative, quantitative, good) specified in the caption of Table 1 are defined according to suitable ranges of Δ assumed by comparing theoretical and numerical curves relevant to different percentage RMS deviations.

Rodriguez 2 algorithm is the only one that ensures good agreement in all of the three tests with the chosen time steps (Δt = 0.018 for *simple shear test* and Δt = 0.02 for the remaining test cases).

In *extension-compression* the six methods that ensure qualitative agreement (highlighted in orange) are all affected by the same type of disagreement (Δ roughly equal to 78%). Since such systematic error surely yields the disagreement highlighted in the previous paragraph for the traction load case of the benchmark problem, it will be investigated in detail in the next section. *Gadala-Wang nonlinear* method yields perfect agreement (Δ nearly equal to 0%) in *extension-compression* test. Among classic methods *Bathe* and *Bathe linear* algorithms accurately agree with theory in simple shear test when σ_{xy} and σ_y stress components are concerned. Nevertheless, their σ_x stress outcome is always zero, so that the relevant total deviation Δ is 100% in shear test. The CC method based on Green-Naghdi stress rate that employs ${}^{t+\Delta t/2}\Delta F^{t+\Delta t}$ deformation gradient (*mid-step Green-Naghdi*) yields better agreement with *exact theory* than the other one when rotations are involved.

3.3 Error in assessment of stress in extension path

The systematic 78% error identified in Table 1 relevant to extension/compression loading conditions (without material rotations) concerns all of the methods exploiting Green-Naghdi objective stress rate (e.g. *Hughes-Green-Naghdi*) as well as Bathe algorithms (referred to as *Bathe linear* and *Bathe*). In addition, the same behavior is observed when Zaremba-Jaumann stress rate

is employed with constant elasticity matrix (*constant C* suffix), e.g. for *Hughes-Winget (constant C)* or *Hughes-Zaremba-Jaumann (constant C)* methods.

Such analogous response of those numerical algorithms is consistent, since they all predict the incremental stress by means of the same rule, which in general is expressed by

$$\boldsymbol{\Delta\sigma} = {}^{t}\mathbf{C} : \boldsymbol{\Delta E}_{m} \tag{2}$$

where ${}^{t}\mathbf{C}$ is the constant elasticity matrix and the measure of the deformation increment $\boldsymbol{\Delta E}_{m}$, according to the specific algorithm, can be referred to: the Green Lagrange strain ($\boldsymbol{\Delta E}_{m} = \boldsymbol{\Delta E}$); the linearized strain ($\boldsymbol{\Delta E}_{m} = \Delta\boldsymbol{\varepsilon}$); the linearized or logarithmic strain computed at half time step ($\boldsymbol{\Delta E}_{m} = {}^{t+\Delta t/2}\Delta\boldsymbol{\varepsilon}$).

Indeed, since no rotations occur, Equation (2) can be approximated if the expression of either Green-Naghdi or Zaremba-Jaumann stress rates (with zero material rotation velocity as well as spin) is multiplied by Δt and substituted into the constitutive relation in incremental form. Indeed, since Green-Naghdi rate is a non-work-conjugate stress rate, an energetically consistent elasticity tensor cannot be found and the spatial (constant) ${}^{t}\mathbf{C}$ one is used in Eq. (2). Similarly, the incremental stress update used in Bathe algorithms basically coincide with Eq. (2), as such methods are coupled with Truesdell rate of Cauchy stress and, again, constant elasticity is considered.

In order to understand the described systematically inaccurate numerical behavior, a *uniaxial extension* test is considered for the sake of more simplicity. In such case, the analytical solution of the inconsistent constitutive equations can be found as explained hereafter, where **L** denotes the spatial gradient of velocity, **D** the deformation rate, **W** is the spin tensor. To this goal, by taking advantage of Biezeno rate of Cauchy stress

$$\boldsymbol{\sigma}'^{(BC)} = \boldsymbol{\sigma}' + \mathrm{Tr}(\mathbf{L})\,\boldsymbol{\sigma} + \boldsymbol{\sigma}\,\mathbf{W} - \mathbf{W}\,\boldsymbol{\sigma} \tag{3}$$

the energetically consistent constitutive equation in Eulerian form can be expressed for a deformation path with no rotations ($\mathbf{W} = \mathbf{0}$) as

$$\boldsymbol{\sigma}' = \mathbf{C}^{(BC)} : \mathbf{D} - \mathrm{Tr}(\mathbf{L})\,\boldsymbol{\sigma} \tag{4}$$

where $\mathbf{C}^{(BC)}$ is the elasticity matrix consistent with Biezeno rate of Cauchy stress [7].

The solution of Eq. (4) due to its consistency coincides with the exact one reported in [12] together with the definition of the deformation path for the *uniaxial extension* test. Differently, in order to simulate the above-described inconsistency, Equation (4) is modified in that the constant elasticity matrix ${}^{t}\mathbf{C}$ is used as substitute for the consistent matrix $\mathbf{C}^{(BC)}$ and the rate of a proper strain measure $\mathbf{E}_{avg}$ replaces the deformation rate **D** as well as the spatial gradient of velocity **L** as follows

$$\boldsymbol{\sigma}' = {}^{t}\mathbf{C} : \mathbf{E}'_{avg} - \mathrm{Tr}(\mathbf{E}'_{avg})\,\boldsymbol{\sigma} \tag{5}$$

The numerical behavior of inconsistent models *weakly* depends on the choice of the particular integration scheme (Euler scheme or mid-point rule) or strain measure (linearized strain, Green-Lagrange, logarithmic) used in the incremental Lagrangian procedure, since for all the tested combinations of these elements the systematic error varies only slightly (see Table 1). Therefore, in the Eulerian Eq. (5) an average strain rate $\mathbf{E'}_{avg} = \{1+t/2,\ 0,\ 0\}^{T}$ is assumed so that the component in the load direction is the average between the linearized and the Green-Lagrange strain rate values (1 and 1+*t*, respectively).

The inconsistent constitutive model expressed by Eq. (5) can be also obtained by means of an alternate procedure that takes advantage of Jaumann stress rate and the relevant elasticity matrix $\mathbf{C}^{(JC)}$. In such case, substituting the definition of Zaremba-Jaumann rate of Cauchy stress with zero spin in the Eulerian constitutive equation consistent with JC stress rate yields

$$\boldsymbol{\sigma}' = \mathbf{C}^{(JC)} : \mathbf{D} = \left(\mathbf{C}^{(BC)} - \mathbf{C}_2\right) : \mathbf{D} = \left({}^{t}\mathbf{C} + \mathbf{C}_1 - \mathbf{C}_2\right) : \mathbf{D} \tag{6}$$

where the components of tensors $\mathbf{C_1}$ and $\mathbf{C_2}$ can be retrieved from expression of consistent elasticity tensors [7].

The inconsistent equation can be found by replacing $\mathbf{D}$ with $\mathbf{E}_{avg}'$ and neglecting $\mathbf{C_1}$ in Eq. (6). Indeed, the latter operation is equivalent to substitute ${}^{t}\mathbf{C}$ for $\mathbf{C}^{(BC)}$ as done in the previous procedure. Therefore, the alternate expression of the inconsistent constitutive equation (Eq. (5)) is

$$\boldsymbol{\sigma}' = \left({}^{t}\mathbf{C} - \mathbf{C}_2\right) : \mathbf{E}'_{avg} \tag{7}$$

Equations (5) and (7) make up the same inconsistent differential problem, when infinitesimals of order higher than the second are neglected. They are both formulated by altering the elasticity tensor consistent with a stress rate that allows to impose zero rotations. Precisely, such stress rate is Biezeno rather than Zaremba-Jaumann, since the Jaumann rate of Cauchy stress is not energetically conjugate to any strain measure [7]. For the plane stress problem at the hand, solving the three differential equations composing Eq. (5) or, equivalently, Eq. (7) with null initial conditions yields the unknown stress components for the *inconsistent theory*

$$\left.\begin{aligned} \sigma_x &= \frac{E}{1-\nu^2}\left[1 - e^{-\left(t+\frac{t^2}{4}\right)}\right] \\ \sigma_{xy} &= 0 \\ \sigma_y &= \frac{E\nu}{1-\nu^2}\left[1 - e^{-\left(t+\frac{t^2}{4}\right)}\right] \end{aligned}\right\} \tag{8}$$

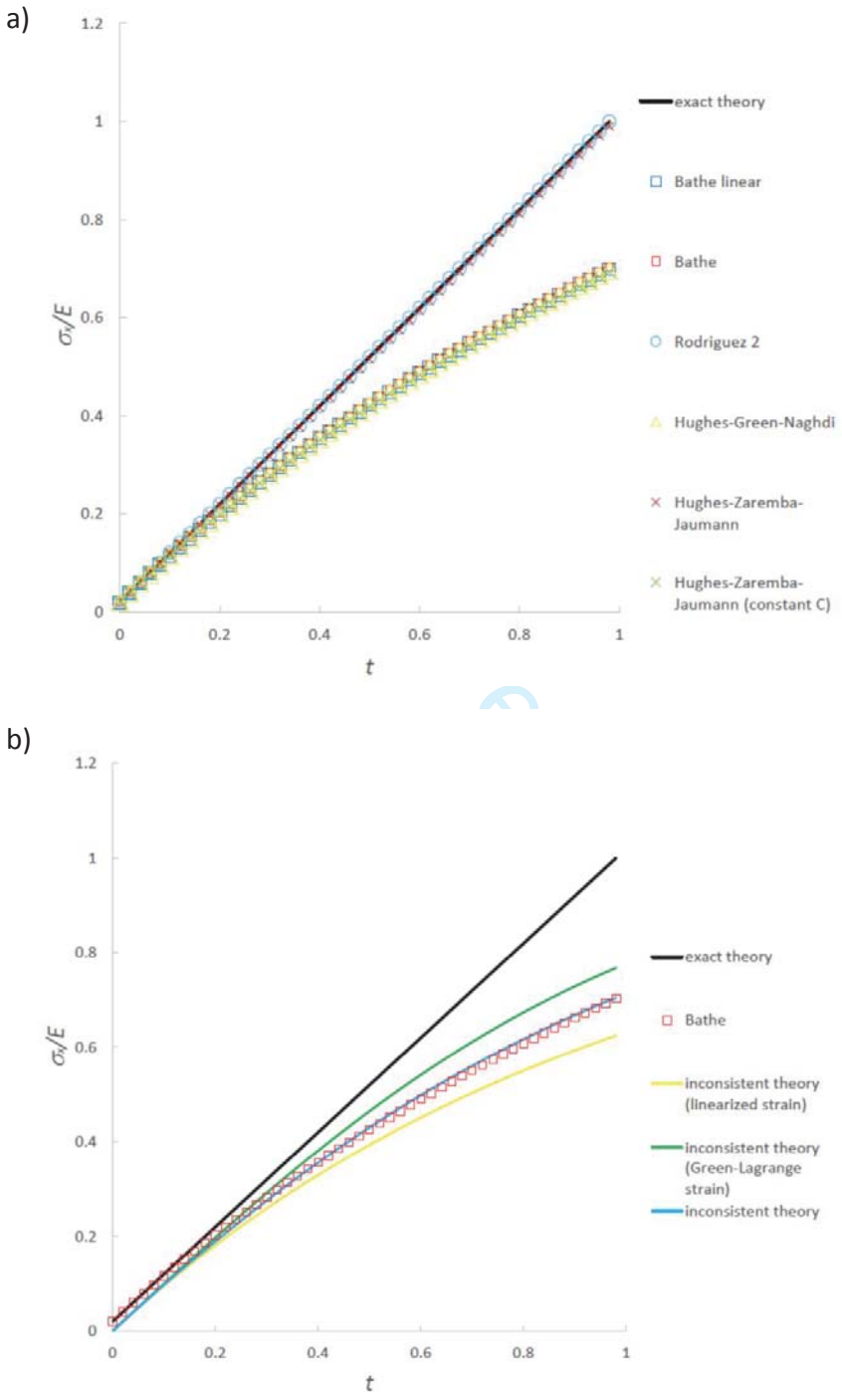

Fig. 4 Stress history of σ_x component predicted by different models for uniaxial extension test: a) comparison among numerical models; b) comparison with different theories.

Fig. 4 shows numerical and analytical stress histories computed for the *uniaxial extension* case. Only σ_x components are plotted since the remaining are always zero for both numerical and analytical models (since $\nu = 0$, no necking occurs). Particularly, Fig. 4 a) compares the stress

computed by some of the inconsistent numerical models cited above and two methods unaffected by the systematic error, i.e. *Rodriguez 2* and *Hughes-Zaremba-Jaumann*. The inconsistent trends are almost overlapped, as already observed for the *extension-compression* test, where the variation among errors Δ of inconsistent models is lower than 3%.

Differently, Fig. 4 b) plots an inconsistent numerical trend, e.g. the one computed by means of *Bathe* method, together with the theoretical curves relevant to the *inconsistent theory*, in order to show the good agreement. Obviously, the theoretical model response depends perceivably on the choice of the strain measure. In any case, the numerical results have always as lower and higher bounds the theoretical trends computed by means of linearized and Green-Lagrange strains, respectively referred to as *inconsistent theory (linearized strain)* and *inconsistent theory (Green-Lagrange strain)*.

3.4 "True" solution of the benchmark problem

For the two load cases of the benchmark problem defined at Paragraph 3.1, Fig. 2 and Fig. 3 compare the main results (stress range and maximum displacements) assessed by means of both commercial software and the in-house developed code *FEMLub*. Particularly, since the latter results are obtained by using *Rodriguez 2* stress integration algorithm, they are assumed as "true" results.

For the traction load case (Fig. 2) the results of *software C* are very close to the "true" solution. Such finding was predictable since *software C* takes advantage of Truesdell stress rate similarly to *Rodriguez 2* algorithm. Mostly due to the inconsistency in stress prediction described in Paragraph 3.3, in the benchmark problem with assigned traction load the relative variation (computed by choosing a reference value equal to the "true" result) between maximum displacements predicted by the different codes is equal to 65.5 %, corresponding to a relative variation in maximum Von Mises stress equal to 35.2 %.

Differently, in the bending load case (Fig. 3) the same variations are much lower than in the traction load case (15.8 and 21.9 % for maximum displacement and Von Mises stress, respectively), although the external force yields significant rotation of the plate material (about -21 degs). Indeed, due to the considerable deflection and bending stress *software D* does not converge, and higher load would also yield a lack convergence in the remaining models with the standard convergence settings. Lower loads (i.e. F_y = - 6.0 × 10^5 N) that allow *software D* to converge would result in lower relative variations.

3.5 Additional benchmark example: axially loaded cantilever beam

Further proof of the systematical inaccuracy described in Paragraph 3.3 can be found in the example reported in [26] (section 5.6). Indeed, such energetic inconsistency involves the accuracy of the corotational kinematic description, which can be investigated by means of the geometrically nonlinear analysis of an axially loaded cantilever beam repeated hereafter.

The geometry of a cantilever beam, with length L = 5000 mm, depth b = 100 mm, and thickness c = 1000 mm, includes a slight imperfection introduced to simulate Euler buckling. To this goal, the tip of the beam in its initial configuration, i.e. its meshed domain, is displaced from the axis by a small amount (10 mm) in lateral direction. As in the previous benchmarks, the material is assumed isotropic linear elastic (with E = 200 000 MPa, ν = 0.3 in this case).

The perturbed geometry of the cantilever beam, the relevant mesh (100 × 2 elements) and constraints are plotted in Fig. 5 together with the relevant static scheme. Since for such perturbation and boundary conditions the effective length factor is K = 1, the analytical Euler buckling load is computed as $p^2 E I / (K L)^2$ = 6.580 × 10^6 N, where I is the minimum area moment of inertia of the cross section of the beam.

Fig. 5 shows that the tip of the cantilever beam (its right end), free to move in vertical direction (DOF u_y is unconstrained), is compressed by an axial displacement u_t, which is uniformly distributed in the tip section, so that it is unable to rotate. Differently, the other end (on the left) is fixed (both u_x and u_y DOFs are blocked).

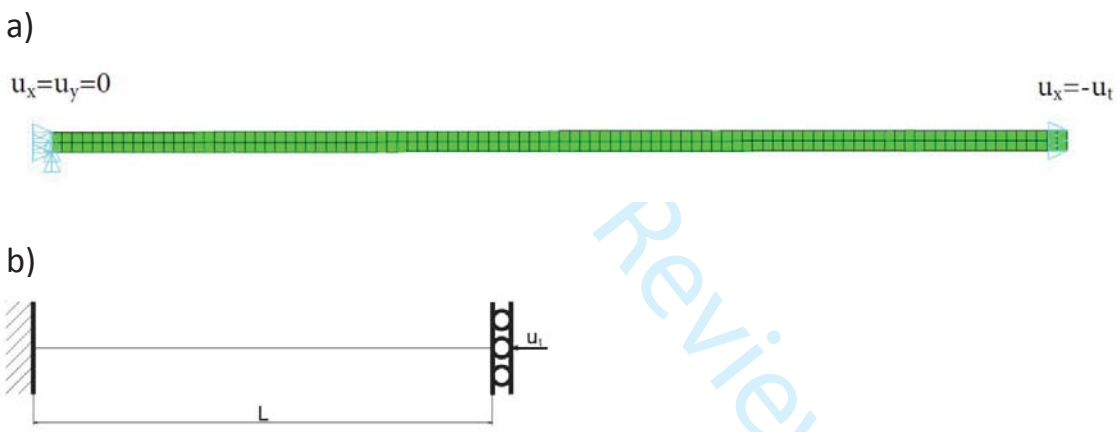

Fig. 5 Axially loaded cantilever beam model: a) perturbed domain mesh and boundary conditions; b) static scheme.

The imposed axial displacement u_t is gradually increased in small steps between 0 and 0.3 mm. Each analysis step assumes as initial stress and displacement those computed in the previous step. Differently, the deformation mode may change abruptly due to the bifurcation and the resulting trend of axial force P vs u_t may be discontinuous.

Such trend is plotted in Fig. 6 for different models, i.e. the analytical Euler model (constant value), large-deflection FEM formulation of *software A* (4 node plane elements with corotational stress as computed in [26]), *software B* (4 node plane elements with B-Bar integration), as well as *FEMLub* code with *Rodriguez 2* stress update algorithm. The models of *software A* and *B* are both affected by the systematic error in study and as expected, give very similar trends which asymptotic values are far away from the analytical solution (relative error in the order of 10%), as already noticed

but not explained in the reference paper for *software A* prediction. On the contrary, the agreement of *Rodriguez 2* stress update algorithm, which is the most accurate in the previous tests and integrates a consistent constitutive equation, provides an asymptotic trend very much closer to Euler buckling load (relative error in the order of 1 %).

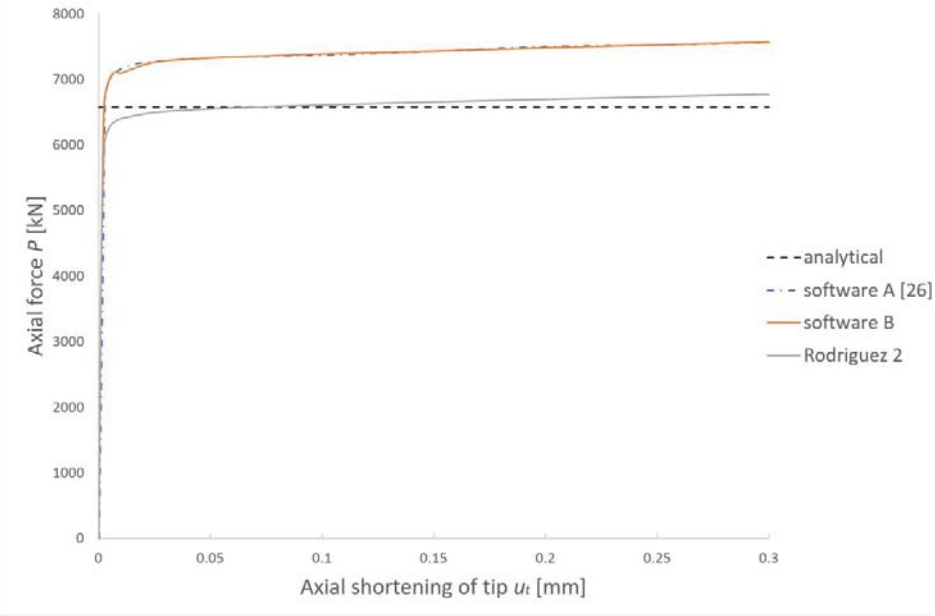

Fig. 6 Axial force P vs displacement u_t of the cantilever beam.

4 Conclusions

The present paper has investigated the most widespread stress update algorithms for FE structural analysis of linear elastic materials including large deformations. A systematic inaccuracy related to traction/compression loading conditions concerns many of the analyzed algorithms. The same differential equation always rules such inaccuracy, so that it causes similar errors in very different algorithms. Such inaccuracy is due to the energetic consistency of the involved models. Particularly, Bazant and Vorel in [17] classify the energy consistence violations in three categories:

1. errors due to the omission of the volumetric terms from objective stress rate.
2. errors due to an inappropriate measure of material rotation.
3. errors caused by a lack in work-conjugacy between objective stress rate and strain tensor, i.e. use of the wrong tangential moduli (elasticity tensor).

The errors of the first type are involved in simulations of highly compressible materials, which are unrelated to the cases considered in the present work. The errors of the second type have been identified by means of *extension-rotation* and *simple shear* tests in some algorithms, e.g. those using Green-Naghdi stress rate. Nevertheless, their influence does not appear to have a substantial impact on the predictions of the presented benchmark simulation, at least for the

traction load-case. According to the current literature [17,18] the third type of errors involves only specific simulations of particular materials, e.g. buckling analysis of highly orthotropic, soft-in-shear materials or shells at small strain. Differently, the present work has demonstrated that such type of errors also affects a usual static analysis when traction/extension loading conditions are involved, namely in most simulations, while it is not limited to materials with specific features. Therefore, such conclusion makes essential the choice of a suitable stress update method for designers that require high accuracy in standard static simulations including large deformations.

Other significant results obtained in the present work are the following:

- the second algorithm proposed in Rodriguez' reference papers [12,13] is the most accurate among the tested integration methods;
- in UL formulations CC methods can achieve incremental objectivity if the current configuration is used as rotation-neutralized configuration and, consequently, incremental rotations are used in order to transform both stress and strain;
- two types of CC methods that use Green-Naghdi stress rate are identified based on the incremental deformation gradient computation;
- the type of CC method that takes advantage of the mid-step configuration and that is devised in the present work performs better than its classic counterpart when rotations are involved in the simulation.

The present work, which deals with generic static simulation problems, yields further arguments that support the same final conclusion as the work presented in [27] about more specific simulation cases, i.e. the commercial codes should replace the adopted corotational stress rates with the Truesdell one conjugated to Green's Lagrange strain.

Acknowledgements

We would like to express our deep gratitude to Professor Alessandro Bottaro for his advice about writing and submitting the paper.

Declaration of Conflicting Interests

The Authors declare that there is no conflict of interest.

Funding

This research received no specific grant from any funding agency in the public, commercial, or not-for-profit sectors.

References

1. Bathe KJ. *Finite Element Procedures*. 2nd ed. Watertown, MA: Prentice Hall, Pearson Education, Inc., http://www.amazon.com/Finite-Element-Procedures-Part-1-

2/dp/0133014584 (1996).
2. Sołowski WT, Hofmann M, Hofstetter G, et al. A comparative study of stress integration methods for the Barcelona Basic Model. *Comput Geotech* 2012; 44: 22–33.
3. Nazem M, Sheng D, Carter JP. Stress integration and mesh refinement for large deformation in geomechanics. *Int J Numer Methods Eng* 2006; 65: 1002–1027.
4. Lee SW, Yoon JW, Yang DY. A stress integration algorithm for plane stress elastoplasticity and its applications to explicit finite element analysis of sheet metal forming processes. *Comput Struct* 1998; 66: 301–311.
5. Hosseini N, Rodríguez-Martínez JA. A simple and computationally efficient stress integration scheme based on numerical approximation of the yield function gradients: Application to advanced yield criteria. *Finite Elem Anal Des*; 192. Epub ahead of print 2021. DOI: 10.1016/j.finel.2021.103538.
6. Choi HS, Yoon JW, Barlat F. Stress update algorithm based on finite difference method and its application to homogenous anisotropic hardening (HAH) model. *J Phys Conf Ser*; 1063. Epub ahead of print 2018. DOI: 10.1088/1742-6596/1063/1/012011.
7. Ji W, Waas AM, Bazant ZP. On the importance of work-conjugacy and objective stress rates in finite deformation incremental finite element analysis. *J Appl Mech Trans ASME* 2013; 80: 1–9.
8. Bathe K-J, Ramm E, Wilson E. Finite element formulations for large deformation dynamic analysis. 1975; 9: 353–386.
9. Hughes TJR, Winget J. Finite rotation effects in numerical integration of rate constitutive equations arising in large-deformation analysis. *Int J Numer Methods Eng* 1980; 15: 1862–1867.
10. Gadala MS, Wang J. Computational implementation of stress integration in FE analysis of elasto-plastic large deformation problems. *Finite Elem Anal Des* 2000; 35: 379–396.
11. Pinsky PM, Ortiz M, Pister KS. Numerical integration of rate constitutive equations in finite deformation analysis. *Comput Methods Appl Mech Eng* 1983; 40: 137–158.
12. Rodriguez-Ferran A, Pegon P, Huerta A. Two Stress Update Algorithms for Large Strains : Accuracy Analysis and Numerical Implementation. *Int J Numer Methods Eng* 1997; 40: 4363–4404.
13. Rodríguez-Ferran A, Huerta A. Comparing two algorithms to add large strains to small-strain FE code. *J Eng Mech* 1998; 124: 939–948.
14. Hughes TJR. Numerical Implementation of Constitutive Models: Rate-Independent Deviatoric Plasticity. *Theor Found large-scale Comput nonlinear Mater Behav* 1984; 29–63.
15. Nagtegaal JC, Veldpaus FE. on the Implementation of Finite Strain Plasticity Equations in a Numerical Model. *Numer Anal Form Process* 1984; 351–371.
16. Aubram D. Notes on rate equations in nonlinear continuum mechanics. 2017; 1–47.
17. Bažant ZP, Vorel J. Energy-conservation error due to use of green-naghdi objective stress rate in commercial finite-element codes and its compensation. *J Appl Mech Trans ASME*; 81. Epub ahead of print 2014. DOI: 10.1115/1.4024411.
18. Ji W, Waas AM, Bazant ZP. Errors Caused by Non-Work Conjugate Stress and Strain Measures and Necessary Corrections in Finite Element Programs. *ASME J Appl Mech*; 77.
19. Bažant ZP. A correlation study of formulations of incremental deformation and stability of continuous bodies. *J Appl Mech Trans ASME* 1971; 38: 919–928.
20. Peter Kohnke. Ansys 15.0 theoretical manual. 2013; 1–988.

21. Griffiths D V., Mustoe GGW. Selective Reduced Integration of Four-Node Plane Element in Closed Form. *J Eng Mech*; 121. Epub ahead of print 1995. DOI: 10.1061/(ASCE)0733-9399(1995)121:6(725).
22. Hughes TJR. Generalization of selective integration procedures to anisotropic and nonlinear media. *Int J Numer Methods Eng* 1980; 15: 1413–1418.
23. Dienes JK. On the analysis of rotation and stress rate in deforming bodies. *Acta Mech* 1979; 32: 217–232.
24. Rashid MM. Incremental kinematics for finite element applications. *Int J Numer Methods Eng* 1993; 36: 3937–3956.
25. Stefani F. Data for the Assessment of Stress Integration Schemes for Large-Deformation Finite Element Analysis. Epub ahead of print 2021. DOI: 10.17632/mx3nj27ddh.1.
26. Mostafa M, Sivaselvan M V., Felippa CA. Reusing linear finite elements in material and geometrically nonlinear analysis - Application to plane stress problems. *Finite Elem Anal Des* 2013; 69: 62–72.
27. Vorel J, Bazant ZP. Review of energy conservation errors in finite element softwares caused by using energy-inconsistent objective stress rates. *Adv Eng Softw* 2014; 72: 3–7.